Towards real-time health monitoring of structural systems via recursive Bayesian filtering and reduced order modelling

Giovanni Capellari

Department of Civil and Environmental Engineering,
Politecnico di Milano,
Piazza L. da Vinci 32, 20133 Milano, Italy
Email: giovanni.capellari@polimi.it

Saeed Eftekhar Azam

Department of Mechanical Engineering,
University of Thessaly,
Leoforos Athinon,
Pedion Areos, 38334 Volos, Greece
Email: eftekhar@uth.gr

Stefano Mariani*

Department of Civil and Environmental Engineering,
Politecnico di Milano,
Piazza L. da Vinci 32, 20133 Milano, Italy
Fax: 02-23994300
Email: stefano.mariani@polimi.it
*Corresponding author

1 Introduction

Civil and industrial structures, exposed to aging and extreme loading conditions, are more and more in need of real-time structural health monitoring (SHM) procedures, immediately able to send out warnings as soon as potentially dangerous situations are approached (Achenbach, 2009).

With a focus on lightweight composite structures and, specifically, on thin laminates (Hull and Clyne, 1996; Reddy, 2004), relevant SHM systems can be designed exploiting sensors of reduced size, that can be embedded in the composite itself, see e.g., Leng and Asundi (2003), Melnykowycz and Brunner (2011) and Konka et al. (2012). But experimental investigations indicate that such embedment can give rise to a local inception of small-scale defects, which represent damage sources at the structural level (Tang et al., 2011). Moving from the pioneering work of Ratcliffe et al. (2008), in Mariani et al. (2013a, 2013c, 2014) and Caimmi et al. (2014) we then proposed a monitoring system consisting of inertial micro-sensors (MEMS), surface-mounted on the structure to sense changes of its response to loading caused by damage events. Experimental results relevant to standard laboratory tests, usually adopted to estimate the inter-laminar strength and toughness of laminates under various loading conditions, already proved that a one-to-one relationship between the sensed motion of the specimen and the location and amount of damage can be obtained.

Besides aspects related to the optimisation of the topology of the network of sensors to be placed over the structure, it has to additionally be ensured that relevant measurements can provide an online estimate of damage; in other words, the sensed change of the structural response has to be distinguishable from noise sources. Moving towards real-time applications, the development of a theoretical/numerical model of the whole structure to govern the monitoring procedure is not an easy task: for instance, in case of composites an accurate structural model needs to allow for micro-scale features possibly causing the inception and growth of damage (see Ladevéze et al., 2006), and so it typically entails high computational costs. Moreover, when damage evolves the system's stiffness and load carrying properties are affected, and so a nonlinear dynamics problem is faced. Procedures to reduce the order of the structural model, like the proper orthogonal decomposition (POD), see e.g., Sirovich (1987), Eftekhar Azam (2014) and Eftekhar Azam and Mariani (2013), prove effective and robust in the linear regime only; to exploit the strengths of POD, in Eftekhar Azam (2014) and Capellari et al. (2016) we proposed to continuously update the sub-space upon which the system evolution equations are projected, taking advantage of the information brought by observations and concerning drifts from the currently estimated structural health. This procedure is discussed in details in this work, and an intricate algorithm centred around a particle-Kalman filter (Kalman, 1960; Arulampalam et al., 2002) and a further Kalman filter is proposed. The former filter is used to estimate the damage pattern in the structure, whereas the latter one is used to tune the projection sub-space.

Results are presented for a thin square plate, supported along its border, loaded by a concentrated force and featuring a uniform damage in regions of its mid-plane. It is reported that, if measurements are collected from sensors deployed according to the proposed optimisation scheme, an accurate estimate of the evolving damage state can be obtained, even when only three degrees-of-freedom are retained in the POD-based reduced-order model governing the filtering procedure.

As the two main topics of sensor deployment and damage identification are here framed within a general approach to SHM, the remainder of the paper is organised as follows. In Section 2, we discuss the optimal deployment of inertial sensors to feel the variation of the local rotation of the mid-plane of the plate, and maximise the overall sensitivity to a damage located anywhere. In Section 3, the estimation of damage location and amount is discussed within an approach driven by the mentioned hybrid particle-Kalman filter. To move towards real-time SHM procedures, in Section 4

a POD-based reduced-order modelling procedure for nonlinear structural dynamics is proposed, and the role of an additional Kalman filter that governs the adaption of the reduced-order model to the changing structural health is detailed. In Section 5, results are reported in terms of optimal placement of the sensors and identification of the partially observed reduced-order system. Finally, some conclusions are provided in Section 6 together with a discussion on possible topics to be addressed in future works.

2 Smart sensing for lightweight structures

As extensively reported in the scientific literature, composite materials are nowadays adopted for lightweight structures thanks to their high stiffness to weight and strength to weight (sometimes also toughness to weight) ratios, see e.g., Hull and Clyne (1996). The other way around, as a mixture of separate materials with different mechanical and thermal properties, the behavioural mismatch at the interfaces between the phases may easily turn into damage processes causing the ultimate failure of the whole structure. Such subtle phenomena are difficult to monitor in case of laminates, made of composite layers stacked one atop the other (Abrate, 1998; Nemat-Nasser and Hori, 1993; Reddy, 2004; Zhuang et al., 2003). As each layer behaves anisotropically due to the specific orientation of elongated inclusions or fibers, a further mismatch of mechanical properties emerges along the inter-laminar surfaces; if layers are differently oriented in the mid-plane of the plate, this latter mismatch may lead to delamination (Allix et al., 1995; Allix et al., 1998; Caiazzo and Costanzo, 2000; Costanzo and Walton, 2002; Yu et al., 2002; Corigliano and Mariani, 2001a, 2001b, 2002; Corigliano and Mariani, 2002; Mariani and Corigliano, 2005). All the resulting damage mechanisms are basically hidden inside the structure; monitoring schemes, able to sense divergence of the current structural response with respect to the perfectly elastic one, are therefore necessary for an effective estimation of damage, see e.g., Bruggi and Mariani (2013) and Mariani et al. (2013a, 2014).

Before addressing the specific problem of damage estimation through the measurements gathered by a network of sensors, a review of some recent results on the optimisation of the topology of the network itself is reported. Exploiting micro-technologies, currently providing cheap commercial off-the-shelf (COTS) inertial MEMS sensors, in Mariani et al. (2013c) and Caimmi et al. (2014) it was proposed to surface-mount such devices so as to avoid any detrimental interaction between them and the composite microstructure, see also Ratcliffe et al. (2008). In fact, when the laminate is produced fibers or other types of sensors (Leng and Asundi, 2003; Mieloszyk et al., 2011; Orlowska et al., 2011; Tang et al., 2011; Minakuchi et al., 2011; Sohn et al., 2011) can be embedded inside the resin-enriched inter-laminar regions between adjacent laminae, but the composite microstructure gets locally distorted, causing defect inception and a reduction of the overall load-carrying capacity or life-time of the structure, see Tang et al. (2011), Butler et al. (2011) and Konka et al. (2012). Surface-mounting the sensors might be dangerous for the SHM system, which is exposed to external agents and to the environment; on the other hand, this approach does not induce any failure mode additional to those caused by loadings only.

The goal of the aforementioned network optimisation approach is thus the deployment over the structure of a given set of inertial sensors, so as to maximise the sensitivity of the SHM system to drifts in the response to loads caused by the

development of damage. In Bruggi and Mariani (2013) and Mariani et al. (2013a), moving from the space-discretised (e.g., through finite elements) model, it was proposed that the topology of the sensor network is optimal if the solution of the following problem is attained:

$$\begin{cases} \max\limits_{x_i} \psi = \displaystyle\sum_{j=1}^{n} \sum_{i=1}^{n} \frac{x_i \|\mathbf{w}_{ji} - \mathbf{w}_i\|}{\max_i x_i \|\mathbf{w}_{ji} - \mathbf{w}_i\|} \\ \text{s.t.} \quad 0 \leq x_i \leq 1 \quad \text{and} \quad \displaystyle\sum_{i=1}^{n} x_i \leq N \end{cases} \tag{1}$$

In equation (1): ψ is the objective function to be maximised; $i = 1, \cdots, n$ is an index running over all the finite elements used in the discretisation of the composite plate; $j = 1, \cdots, n$ is an additional index running once again over all the elements, and used to denote the element where damage is located; $\mathbf{w}_i$ is the structural response to the loading in the undamaged case and at the i^{th} element (since such solution, for computational convenience, is handled in an element-wise fashion), and $\mathbf{w}_{ji}$ is the response to the same loading if damage is located inside the j^{th} element only; $\|\square\|$ indicates the norm of vector $\square$; N is the a-priori defined number of sensors to be deployed; x_i is a discrete variable field, constant inside each element, adopted to denote the presence ($x_i = 1$) or absence ($x_i = 0$) of the sensor on the element itself.

Some of the details of the reasoning to obtain the formulation in equation (1) are discussed now. First of all, the two indices i and j are necessary to decouple where damage is sensed (in the i^{th} element) and where it is located (in the j^{th} element). Although it looks time-consuming to compute the $n + 1$ structural responses $\mathbf{w}_{ji}$ and $\mathbf{w}_i$, the first n ones linked to damage located in one element only (as said, the j^{th} one) and the last one linked instead to the undamaged case, this turns out to be compulsory to assure that the placement of the sensors is optimal no matter what the (unknown) location of damage is. The non-dimensional form of each term summed up in the objective function ψ has been devised to enhance the reliability of the optimisation approach, independently of the loading condition (see Bruggi and Mariani, 2013): without the term at the denominator, which scales all the contributions so that they amount at most to one at assigned damage case, the sensor placement would be moved towards regions maximising extremal values of the contributions $x_i \|\mathbf{w}_{ji} - \mathbf{w}_i\|$, and not the relevant average. From a statistical viewpoint, this result has been considered dangerous for the placement of the sensors, as the overall network sensitivity can be largely smaller than the optimal one if damage gets incepted in a region not providing the mentioned extreme values. Therefore, the approach leading to equation (1) allows to attain a balanced sensitivity to all the foreseen damage events. Concerning the magnitude of damage handled in the analyses providing terms $\mathbf{w}_{ji}$, in Mariani et al. (2013b) it was also shown that it marginally affects the outcome of the optimisation procedure.

As far as the discrete density field x_i is concerned, it has been assumed constant inside each element, which in turn is considered as the smallest portion of the structures that can be monitored. This field can take real values, not only integer ones, in compliance with the constraint $0 \leq x_i \leq 1$; hence, the number N of devices to be deployed does not necessarily turn out to be linked to N locations only. Usually, such locations are more than N as (at least) some x_i values are smaller than one. In Bruggi

and Mariani (2013), some algorithmic strategies were discussed to add a penalisation for the intermediate densities, and so tend to almost purely 0-1 solutions; readers are referred to that paper for all the computational details and relevant theoretical setting.

As stated here above, the characteristic element size is considered to be the smallest possible resolution of the optimisation scheme and, therefore, of the SHM approach to be detailed in what follows. In the analysis, it must be anyway borne in mind that three length-scales should be accounted for: the first scale, to be considered as the macroscopic one, is linked to the structural geometry and the spatial variation of the loadings, and can be for instance assumed coincident with any in-plane dimension L of the composite plate; the second scale, the mesoscopic one (see Ladevéze et al., 2006), is linked to the size of the region where damage can be incepted and so, granted that a coarse-grained discretisation of the structure proves sufficient for the SHM purposes, to the characteristic size l of the finite elements; the third, microscopic scale is finally linked to the size ℓ of the MEMS devices to be placed over the laminate. In standard situations, L and ℓ can differ by two-three orders of magnitude; a multi-scale approach thus looks necessary to catch all the mesoscopic details of the structural health, and to also provide an effective placement of the micro-sensors. Along this line, a decoupled multi-scale approach was proposed in Mariani et al. (2013b) and will be further developed in future investigations.

As for the type of sensors to be adopted in the SHM procedure to sense the responses $\mathbf{w}_{ji}$ and $\mathbf{w}_i$ to loading, the kinematics of thin composite plates has been accounted for, and so both translational and rotational degrees-of-freedom can be handled in the said vectors. Assuming that load can only induce small deformations of the structure, the kinematic variables in $\mathbf{w}_{ji}$ and $\mathbf{w}_i$ turn out to be the out-of-plane deflection, and the two rotations about the in-plane axes of any reference frame. Concerning the inertial sensors to be deployed over the structure, in Mariani et al. (2013a, 2014) it was already reported that a sensing of the rotation about the in-plane axes is preferable to the sensing of the out-of-plane deflection for two main reasons. First, close to the borders of the plate, where the motion is typically constrained, the deflection is zero or so small that it cannot be detected with COTS sensors; these regions are on the other hand extremely dangerous as for the mentioned delamination events, since the heterogeneity and anisotropy of the composite can lead to local stress intensifications, see O'Brien (1984) and Corigliano (2003). Second, if rotations are handled both accelerometers and gyroscopes can be adopted as sensors: gyroscopes are targeted to sense rotational motions, but accelerometers can be also used since they are designed to feel their orientation relative to the vertical (gravity) direction. Hence, rotations inducing a variation of the sensed components of the gravity field can be exploited in statics (not only in dynamics) to monitor the health of thin plates.

3 Dual estimation of partially observed nonlinear systems

We discuss now a general scheme for the estimation of quantities of interest in a structural system, driven by data brought by the sensors deployed over the structure. As damage indices and further model parameters are not directly measurable, an appropriate signal processing method is required to extract meaningful information from the measurements. Due to economical and also technical reasons, it is often desirable to use as few measurement devices as possible; the entire state of the system is accordingly

hidden, or only partially observable. Furthermore, a physical model is needed to relate the whole state of the system to its observable part; it often turns out that inaccuracies of the physical model and of the measurements cannot be neglected, and the signal processing procedure has to systematically account for them.

Within a stochastic frame, the full state of a partially observed system is here estimated through a recursive Bayesian filter. Making reference to a linear discrete system, after having partitioned the time interval of interest according to $[t_0 \quad t_{end}] = \cup_{k=1}^{N_t}[t_{k-1} \quad t_k]$ its state-space model reads:

$$\mathbf{x}_k = \mathbf{A}(\boldsymbol{\vartheta}, \boldsymbol{\varphi})\mathbf{x}_{k-1} + \mathbf{B}\mathbf{u}_{k-1} + \mathbf{v}_k^x \tag{2}$$

$$\mathbf{y}_k = \mathbf{C}(\boldsymbol{\varphi})\mathbf{x}_k + \mathbf{D}\mathbf{u}_{k-1} + \mathbf{v}_k^y \tag{3}$$

where $\mathbf{x}_k$ stands for the whole state of the system at time instant t_k; $\mathbf{y}_k$ is the observation process at the same time t_k; $\mathbf{u}_{k-1}$ denotes the known input to the system at t_{k-1}; terms $\mathbf{v}_k^x$ and $\mathbf{v}_k^y$ define the uncertainties in the process and observation equations, respectively featuring time-invariant covariances $\mathbf{V}^x$ and $\mathbf{V}^y$; vectors $\boldsymbol{\vartheta}$ and $\boldsymbol{\varphi}$ are two sets of model parameters in need of estimation; $\mathbf{A}(\boldsymbol{\vartheta}, \boldsymbol{\varphi})$ maps the state of the system within the discrete time interval $[t_{k-1} \quad t_k]$, and is a function of the parameters of the physical model gathered in $\boldsymbol{\vartheta}$ and $\boldsymbol{\varphi}$; $\mathbf{B}$ links the input to the system and its state, and so does the transmission matrix $\mathbf{D}$ as far as observations are concerned; $\mathbf{C}(\boldsymbol{\varphi})$ stands for the relation between the state of the system and the observation process, and is here supposed to be a function of the vector $\boldsymbol{\varphi}$. In equation (2), system parameters are arranged into the two different sets $\boldsymbol{\vartheta}$ and $\boldsymbol{\varphi}$ to allow for a specific physical interpretation: while parameters in $\boldsymbol{\vartheta}$ represent uncertainties in the model related to the real behaviour of the structure, which is typically known up to a few parameters in need of fine tuning, parameters in $\boldsymbol{\varphi}$ are supposed to come from a possible reduced-order modelling procedure (as described in Section 4). Accordingly, the parameters are handled in a disjoint fashion, as the latter set is related to the computational SHM approach and not explicitly to the material or structural behaviour.

Table 1 Kalman filter algorithm

1 Initialisation at time t_0:
- $\hat{\mathbf{x}}_0 = \mathbb{E}[\mathbf{x}_0]$
- $\mathbf{P}_0 = \mathbb{E}[(\mathbf{x}_0 - \hat{\mathbf{x}}_0)(\mathbf{x}_0 - \hat{\mathbf{x}}_0)^{\mathrm{T}}]$

2 At time t_k, for $k = 1, ..., N_t$:
- a Prediction stage
  - 1 Evolution of state and prediction of covariance
    - $\mathbf{x}_k^- = \mathbf{A}\mathbf{x}_{k-1} + \mathbf{B}\mathbf{u}_{k-1}$
    - $\mathbf{P}_k^- = \mathbf{A}\mathbf{P}_{k-1}\mathbf{A}^{\mathrm{T}} + \mathbf{V}^x$
- b Update stage
  - 1 Calculation of Kalman gain
    - $\mathbf{G}_k = \mathbf{P}_k^-\mathbf{C}^{\mathrm{T}}(\mathbf{C}\mathbf{P}_k^-\mathbf{C}^{\mathrm{T}} + \mathbf{V}^y)^{-1}$
  - 2 Improve predictions using the latest observations
    - $\hat{\mathbf{x}}_k = \mathbf{x}_k^- + \mathbf{G}_k(\mathbf{y}_k - \mathbf{C}\mathbf{x}_k^- - \mathbf{D}\mathbf{u}_{k-1})$
    - $\mathbf{P}_k = \mathbf{P}_k^- - \mathbf{G}_k\mathbf{C}\mathbf{P}_k^-$

If the process and observation noises $\mathbf{v}_k^x$ and $\mathbf{v}_k^y$ are white and Gaussian, the Kalman filter provides an optimal online estimate for the state of the system, upon availability of the observation process $\mathbf{y}_k$ (Kalman, 1960; Gelb, 1974). Table 1 collects the algorithmic details of the Kalman filter. It can be seen that the algorithm is started with an initial guess for the expected values of mean and covariance of the state; after this initialisation step, the filter consists in a prediction stage, which is simply an evolution of the state over time, and in an update stage. In the latter stage, through the Kalman gain $\mathbf{G}_k$ the filter enhances the currently predicted value of $\mathbf{x}_k$.

In what precedes, it has been assumed that the mapping matrices of the system are time-invariant due to the linear (namely, elastic) structural behaviour. In a general case featuring damage evolution, the parameters in $\boldsymbol{\vartheta}$ and $\boldsymbol{\varphi}$ can also evolve in time. In such a case the state of the system is augmented according to $\mathbf{z}_k = \{\mathbf{x}_k \quad \boldsymbol{\vartheta}_k \quad \boldsymbol{\varphi}_k\}^{\mathrm{T}}$, and a recursive Bayesian filter is still adopted to improve the estimates of the whole state when new observations become available. In doing so, the following equation is further considered in the state-space model:

$$\begin{Bmatrix} \boldsymbol{\vartheta}_k \\ \boldsymbol{\varphi}_k \end{Bmatrix} = \begin{Bmatrix} \boldsymbol{\vartheta}_{k-1} \\ \boldsymbol{\varphi}_{k-1} \end{Bmatrix} + \begin{Bmatrix} \mathbf{v}_k^{\vartheta} \\ \mathbf{v}_k^{\varphi} \end{Bmatrix} \tag{4}$$

where it is assumed that both $\boldsymbol{\vartheta}$ and $\boldsymbol{\varphi}$ can evolve in time following random walks, with relevant fictitious noise contributions $\mathbf{v}_k^{\vartheta}$ and $\mathbf{v}_k^{\varphi}$. The theoretical background for equation (4) was extensively discussed in Eftekhar Azam (2014) and Capellari et al. (2016); basically, it implies that even if damage evolves, and so the system response and the parameters describing it evolve as well, such evolution is smooth and slow enough so that it can be considered a piece-wise constant process. Accordingly, also the reduced-order model, coming into play through the vector $\boldsymbol{\varphi}_k$, has to be progressively updated in a piece-wise constant mode. Such reasoning is linked to a kind of time-scales separation principle: if the characteristic times corresponding to system evolution (the fast one) and to damage evolution (the slow one) are well-separated, within each time step the damage state and the corresponding parameters in $\boldsymbol{\vartheta}_k$ and $\boldsymbol{\varphi}_k$ can be assumed constant.

By gathering all the state-space equations together, the following dual formulation is arrived at:

$$\begin{Bmatrix} \mathbf{x}_k \\ \boldsymbol{\vartheta}_k \\ \boldsymbol{\varphi}_k \end{Bmatrix} = \begin{Bmatrix} \mathbf{A}(\boldsymbol{\vartheta}_{k-1}, \boldsymbol{\varphi}_{k-1}) & \mathbf{0} & \mathbf{0} \\ \mathbf{0} & \mathbf{I} & \mathbf{0} \\ \mathbf{0} & \mathbf{0} & \mathbf{I} \end{Bmatrix} \begin{Bmatrix} \mathbf{x}_{k-1} \\ \boldsymbol{\vartheta}_{k-1} \\ \boldsymbol{\varphi}_{k-1} \end{Bmatrix} + \begin{Bmatrix} \mathbf{B}\mathbf{u}_{k-1} \\ \mathbf{0} \\ \mathbf{0} \end{Bmatrix} + \begin{Bmatrix} \mathbf{v}_k^x \\ \mathbf{v}_k^{\vartheta} \\ \mathbf{v}_k^{\varphi} \end{Bmatrix} \tag{5}$$

$$\mathbf{y}_k = \begin{bmatrix} \mathbf{C}(\boldsymbol{\varphi}_k) & \mathbf{0} & \mathbf{0} \end{bmatrix} \begin{Bmatrix} \mathbf{x}_k \\ \boldsymbol{\vartheta}_k \\ \boldsymbol{\varphi}_k \end{Bmatrix} + \mathbf{D}\mathbf{u}_{k-1} + \mathbf{v}_k^y \tag{6}$$

where nonlinearities stem first of all by the (either implicit or explicit) dependence of the mapping matrices $\mathbf{A}$ and $\mathbf{C}$ on vectors $\boldsymbol{\vartheta}$ and $\boldsymbol{\varphi}$. In the cases here envisioned, one has to deal with further sources of nonlinearities linked to the inception and subsequent evolution of damage.

An optimal estimation of the whole state $\mathbf{z}_k$ of nonlinear systems is in general not possible, and a recursive Bayesian filter [like e.g., the extended Kalman filter (EKF), the unscented Kalman filter (UKF) or a particle filter] must be employed to obtain

sub-optimal estimates, see e.g., Eftekhar Azam (2014). In fact, with the so-called EKF the Kalman filtering scheme is used at each recursion for a linearised version of the nonlinear model equations (Gelb, 1974; Mariani and Corigliano, 2005). In the presence of severe nonlinearities, the EKF can lead to substantial errors. To alleviate such issue, in Julier et al. (1995, 2000) the use of the so-called unscented transform was proposed to generate a set of deterministic, particle-like realisations of the system, to be evolved in time according to the actual nonlinear model; this approach provided the basis of the UKF.

The aforementioned methods use the Kalman filter as back-bone, and perform well as long as the basic assumptions of the Kalman filter are not violated much. For instance, the EKF can deliver relatively accurate estimates when the probability distribution function (PDF) of the state vector is close to a Gaussian one. The UKF was designed to outperform the EKF in the presence of skewness in the PDF of the state but, in case this turns out to be bimodal, also this filter fails to deliver accurate estimates. In response to such shortcomings, particle filtering was proposed in order to deal with problems with general PDFs, and so to attack cases featuring nonlinearly evolving non-Gaussian distributions (Arulampalam et al., 2002). Within such frame, a Monte Carlo method is used to numerically handle the Chapman-Kolmogorov integral equation; but, when dealing with high-dimensional multivariate problems, the computational demand of this approach prevents its real-time application. To mitigate all the mentioned issues, in Eftekhar Azam and Mariani (2012) an EKF-enhanced particle filter scheme was adopted wherein the drawn particles are pushed towards the regions (in the PDF space) of high probability by an EKF, see Table 2. At variance with what reported in Table 1, with this approach a set of N_p particles $\mathbf{x}_k^{(i)}$ is drawn from the beginning of the filtering procedure, each one associated with a covariance matrix $\mathbf{P}_k^{(i)}$ and a weight $\omega_k^{(i)}$. Information brought by all the particles are merged at the end of each time step to move forward the estimate $\hat{\mathbf{x}}_k$ of the state (and the relevant covariance, although not reported for brevity in Table 2). The drawing of the particles and the evolution of the relevant weights can thus account for the mentioned non-Gaussianity of the system PDF. Due to the nonlinear evolution of the system, mappings **A** and **C** become time- and state-dependent, so they are reported in Table 2 with the index k referring to the time instant t_k.

The variance of the importance weights $\omega_k^{(i)}$ is known to increase stochastically over time (Doucet et al., 2000), so that after a few time steps most of them or even all but one tend to zero. This issue is referred to as sample degeneracy. To alleviate it, a resampling stage may be used to eliminate samples with low importance weights and duplicate samples with high importance. Several methods have been proposed to cope with that, like e.g., multinomial, stratified, systematic and residual resampling schemes; differences among them lie on the criterion adopted to distinguish high and low importance weights. In Chatzi and Smyth (2009) and Chatzi and Smyth (2013) a Gaussian mixture sigma-point particle filter and a particle filter with mutation were respectively adopted; here, systematic resampling is instead exploited, due to its low computational complexity in comparison with the above mentioned methods, see Hol et al. (2006). It must be noted that such approach is sensitive to the order in which particles are sorted; switches among them changes the particle distribution, and therefore an analytical study of the algorithmic performance becomes difficult, see Douc and Cappe (2005).

Table 2 Hybrid particle-Kalman filter algorithm

1 Initialisation at time t_0, for $i = 1, ..., N_p$:
$\hat{\mathbf{x}}_0 = \mathbb{E}[\mathbf{x}_0]$
$\mathbf{P}_0 = \mathbb{E}[(\mathbf{x}_0 - \hat{\mathbf{x}}_0)(\mathbf{x}_0 - \hat{\mathbf{x}}_0])^{\mathrm{T}}]$
$\mathbf{x}_0^{(i)} = \hat{\mathbf{x}}_0$
$\omega_0^{(i)} = p(\mathbf{y}_0|\mathbf{x}_0)$
$\mathbf{P}_0^{(i)} = \mathbf{P}_0$

2 At time t_k, for $k = 1, ..., N_t$ and $i = 1, ..., N_p$:

a Prediction stage

1 Draw particles
$\mathbf{x}_k^{(i)-} \sim p(\hat{\mathbf{x}}_k|\mathbf{x}_{k-1}^{(i)})$

2 Push particles toward the region of high probability through an EKF
$\mathbf{P}_k^{(i)-} = \mathbf{A}_k \mathbf{P}_{k-1}^{(i)} \mathbf{A}_k^{\mathrm{T}} + \mathbf{V}^x$
$\mathbf{G}_k^{(i)} = \mathbf{P}_k^{(i)-} \mathbf{C}_k^{\mathrm{T}} (\mathbf{C}_k \mathbf{P}_k^{(i)-} \mathbf{C}_k^{\mathrm{T}} + \mathbf{V}^y)^{-1}$
$\mathbf{x}_k^{(i)} = \mathbf{x}_k^{(i)-} + \mathbf{G}_k^{(i)} (\mathbf{y}_k - \mathbf{C}_k \mathbf{x}_k^{(i)-} - \mathbf{D}\mathbf{u}_{k-1})$
$\mathbf{P}_k^{(i)} = \mathbf{P}_k^{(i)-} - \mathbf{G}_k^{(i)} \mathbf{C}_k \mathbf{P}_k^{(i)-}$

b Update stage

1 Evolve weights
$\omega_k^{(i)} = \omega_{k-1}^{(i)} p(\mathbf{y}_k|\mathbf{x}_k^{(i)})$

2 Resampling, see Eftekhar Azam (2014) and Capellari et al. (2016)

3 Compute expected value and other required statistics
$\hat{\mathbf{x}}_k = \sum_{i=1}^{N_p} \omega_k^{(i)} \mathbf{x}_k^{(i)}$

A further computational problem is considered next. One challenge, affecting all the schemes dealing with parameter identification, is the so-called curse of dimensionality: if the number of parameters to be estimated becomes large, the accuracy of the results is decreased and the filters can furnish biased estimates. To alleviate this issue, the parameter identification task is split into two stages. As mapping $\mathbf{C}$ is assumed to be a linear function of its argument $\boldsymbol{\varphi}_k$, the observation equation (3) is reformulated as follows:

$$\mathbf{y}_k = \mathbf{C}^{\boldsymbol{\varphi}}(\mathbf{x}_k)\boldsymbol{\varphi}_k + \mathbf{D}\mathbf{u}_{k-1} + \mathbf{v}_k^y \tag{7}$$

Equations (4_2) and (7) then provide a set of linear state-space equations; in a first stage such linearity is exploited to provide a nearly optimal solution for the vector $\boldsymbol{\varphi}_k$ through a Kalman filter. In a second stage, the state-space equations dealt with by the hybrid particle-Kalman filter become:

$$\begin{Bmatrix} \mathbf{x}_k \\ \boldsymbol{\vartheta}_k \end{Bmatrix} = \begin{Bmatrix} \mathbf{A}(\boldsymbol{\vartheta}_{k-1}, \hat{\boldsymbol{\varphi}}_{k-1}) & \mathbf{0} \\ \mathbf{0} & \mathbf{I} \end{Bmatrix} \begin{Bmatrix} \mathbf{x}_{k-1} \\ \boldsymbol{\vartheta}_{k-1} \end{Bmatrix} + \begin{Bmatrix} \mathbf{B}\mathbf{u}_{k-1} \\ \mathbf{0} \end{Bmatrix} + \begin{Bmatrix} \mathbf{v}_k^x \\ \mathbf{v}_k^{\vartheta} \end{Bmatrix} \tag{8}$$

$$\mathbf{y}_k = \begin{bmatrix} \mathbf{C}(\hat{\boldsymbol{\varphi}}_{k-1}) & \mathbf{0} \end{bmatrix} \begin{Bmatrix} \mathbf{x}_k \\ \boldsymbol{\vartheta}_k \end{Bmatrix} + \mathbf{D}\mathbf{u}_{k-1} + \mathbf{v}_k^y \tag{9}$$

where $\hat{\boldsymbol{\varphi}}_{k-1}$ stands for the estimated value of the vector at the beginning of the time step, i.e., just before the new update.

4 Towards real-time SHM of complex structures

It has been already emphasised that local damage processes in lightweight composite structures need accurate models to be identified through the envisioned SHM procedure. Therefore, the number of degrees-of-freedom typically adopted in relevant space discretisations prevents any procedure to work in real-time. We now exploit the formulation provided in Section 3, where two different sets of parameters to be identified were retained in the expanded state vector $\mathbf{z}_k$, to propose an adaptive reduced-order modelling procedure formerly developed for linear systems only.

The formulation is tailored to locate and quantify a damage in the structure. Following a rather standard approach, damage parameters are associated to a local reduction of the structural stiffness only; for simplicity, damage is also supposed to develop isotropically. By subdividing the whole structure into N_z non-overlapping sub-domains, each one is associated with a damage index d_{i} that scales the corresponding Young's modulus E as follows:

$$E_{\mathsf{i}} = (1 - d_{\mathsf{i}})E \qquad \mathsf{i} = 1, ..., N_z \tag{10}$$

The assumption of a homogeneous reduction of the mechanical stiffness in each region does not represent a limitation of the procedure; in fact, like in the network optimisation procedure, each zone may consist of one element only, whose characteristic size becomes the resolution scale of the SHM system. More complex damage models can be obviously allowed for, within the present framework.

The algorithm has been devised to apply to any kind of structure, and for any type of discretisation. Exploiting keywords and user interfaces of the commercial finite element code Abaqus, the structural mass and stiffness matrices are obtained and further handled to build the reduced-order model. To properly account for the stiffness contribution coming from each single zone where damage can develop, the overall stiffness matrix $\mathbf{K}$ is assembled according to, see Zienkiewicz and Taylor (2000):

$$\mathbf{K} = \mathbf{A}_{\mathsf{i}=1}^{N_z} \frac{1 - d_{\mathsf{i}}}{1 - \bar{d}} (\mathbf{K}_{und} - \mathbf{K}_{\mathsf{i}}) \tag{11}$$

where $\mathbf{A}$ is the assemblage operator; $\mathbf{K}_{und}$ is the whole structural stiffness matrix in the undamaged configuration; and $\mathbf{K}_{\mathsf{i}}$, $\mathsf{i} = 1, ..., N_z$, is an appropriate auxiliary stiffness contribution relevant to the i-th zone only and linked to a fictitious damage index $\bar{d}$, constant and different from zero only in the said region. Accordingly, the vector $\boldsymbol{\vartheta}_k$ of model parameters to be identified gathers the damage indicators d_{i}, namely:

$$\boldsymbol{\vartheta}_k = \left\{ d_{1,k} \quad ... \quad d_{N_z,k} \right\}^{\mathrm{T}} \tag{12}$$

where the index k is adopted to signify that in the SHM procedure the estimations of the damage indices vary in time, as provided by the hybrid particle-Kalman filter of Table 2.

It has been already pointed out that the main drawback of any identification method based on standard recursive Bayesian filters is represented by the excessive computational costs for real-life situations. To move towards real-time applications, a model order reduction procedure is adopted to reduce the dimensionality of the model,

still maintaining a proper level of accuracy concerning the state variables to be compared with the data coming from measurements. The reduced-order model is obtained through a Galerkin projection of the original, full-order one onto a sub-space provided by POD in its snapshot version (Sirovich, 1987). The bases to perform such projection are the so-called proper orthogonal modes (POMs), set to mimic the experimentally (or pseudo-experimentally, as in Section 5) collected sensor signals.

POD requires an initial training stage of the reduced-order model, whose time duration can be set on-the-fly according to some convergence criteria for the POMs and for the relevant energy content, see Corigliano et al. (2013a, 2013b, 2015). In the said training stage, snapshots of the structural response to the loading are collected; as the structural system is supposed to be only partially observed (see Section 3), the deployment of the sensors has thus to be optimised, e.g., as proposed is Section 2. Depending on the target accuracy of the model, the number o of POMs to be retained can be obtained, see e.g., Eftekhar Azam and Mariani (2013). Within the proposed procedure, these POMs are handled through the vector $\boldsymbol{\varphi}_k$, and can therefore be online updated during monitoring if drifts from the initial health condition are detected by the deployed sensors.

Having defined the order o of the reduced-order model, the structural mass $\mathbf{M}$ and stiffness $\mathbf{K}$ matrices governing system evolution of the linear comparison model, are then projected onto the sub-space spanned by POMs according to:

$$\boldsymbol{\mathcal{M}}_k = \boldsymbol{\Phi}_k^{\mathrm{T}} \mathbf{M} \boldsymbol{\Phi}_k \qquad \boldsymbol{\mathcal{K}}_k = \boldsymbol{\Phi}_k^{\mathrm{T}} \mathbf{K} \boldsymbol{\Phi}_k \tag{13}$$

where $\boldsymbol{\Phi}_k$ is a matrix gathering the current (vector-valued) values or estimates of the retained POMs. Additional details concerning the reduction of the order of the structural model can be found in Eftekhar Azam (2014) and Capellari et al. (2016).

Moving now to the state-space formalism, the state vector $\mathbf{x}_k$ is assumed to read:

$$\mathbf{x}_k = \left\{ \mathbf{w}_k \quad \dot{\mathbf{w}}_k \quad \ddot{\mathbf{w}}_k \right\}^{\mathrm{T}} \tag{14}$$

where not only the kinematic nodal (or elemental, see Section 2) variables $\mathbf{w}_k$ are gathered to define the current configuration of the structure, but also the corresponding time rates $\dot{\mathbf{w}}_k$ and $\ddot{\mathbf{w}}_k$. This shape of the state vector was already reported in Mariani and Ghisi (2007) to be a condition to properly track the evolution of the statistics of the whole system, once nonlinear phenomena take place.

The filter of Section 3 and the reduced-order modelling here detailed have now to be joined together; the mapping and covariance matrices of Table 2 are accordingly affected by the algorithmic procedure adopted. In Figure 1, the proposed algorithm is summarised as a flow chart, where the exogenous input $\mathbf{u}_{k-1}$ has been disregarded for simplicity. The method can be conceptually subdivided into two stages. In the first stage (red box of Figure 1), once the measured signals $\mathbf{y}_k$ are given the state vector is estimated through the hybrid particle-Kalman filter. As system health may evolve in time due to damage development, state equations become nonlinear and do require a linearisation step: mapping $\boldsymbol{\mathcal{A}}_k^{(i)}$ acts here as $\mathbf{A}$ in equation (8) to evolve the $(i)^{\text{th}}$ particle within the reduced-order setting. With a similar notation: $\boldsymbol{\mathcal{X}}_k^{(i)}$ is the current realisation of the reduced-order state vector provided by the $(i)^{\text{th}}$ particle, and gathers all the state contributions but $\boldsymbol{\varphi}_k$ (handled separately in stage 2); $\boldsymbol{\mathcal{P}}_k^{(i)}$ is the relevant covariance matrix; and $\boldsymbol{\mathcal{V}}^x$ is the covariance of the noise in the projected state evolution equations.

Since observations $\mathbf{y}_k$ are linked to the full-oder state vector $\mathbf{x}_k$, see equation (9), when the reduced-order vector $\boldsymbol{\mathcal{X}}_k^{(i)}$ is evolved a matrix $\mathbf{L}_k$ is necessary to return back to the original, full-order observation equation. In accordance with the definition of $\boldsymbol{\mathcal{X}}_k^{(i)}$ reported here above, matrix $\mathbf{L}_k$ reads:

$$\mathbf{L}_k = \begin{bmatrix} \boldsymbol{\Phi}_k & & & \\ & \boldsymbol{\Phi}_k & & \\ & & \boldsymbol{\Phi}_k & \\ & & & \mathbf{0} \end{bmatrix} \tag{15}$$

where the last pivotal (matrix-valued) zero entry means that damage parameters cannot be observed. Weights $\omega_k^{(i)}$ are then evolved in time through the following multivariate Gaussian distribution:

$$p(\mathbf{y}_k|\boldsymbol{\mathcal{X}}_k^{(i)}) = \frac{1}{\sqrt{(2\pi)^n \|\boldsymbol{\mathcal{P}}_{k-1}^{(i)}\|}} \times \exp\left\{-\frac{1}{2}(\mathbf{y}_k - \mathbf{C}_k\mathbf{L}_{k-1}\boldsymbol{\mathcal{X}}_k^{(i)})^{\mathrm{T}}\boldsymbol{\mathcal{P}}_{k-1}^{(i)-1}(\mathbf{y}_k - \mathbf{C}_k\mathbf{L}_{k-1}\boldsymbol{\mathcal{X}}_k^{(i)})\right\} \tag{16}$$

Figure 1 Flow chart of the procedure used for dual estimation of the reduced-order model and sub-space update (see online version for colours)

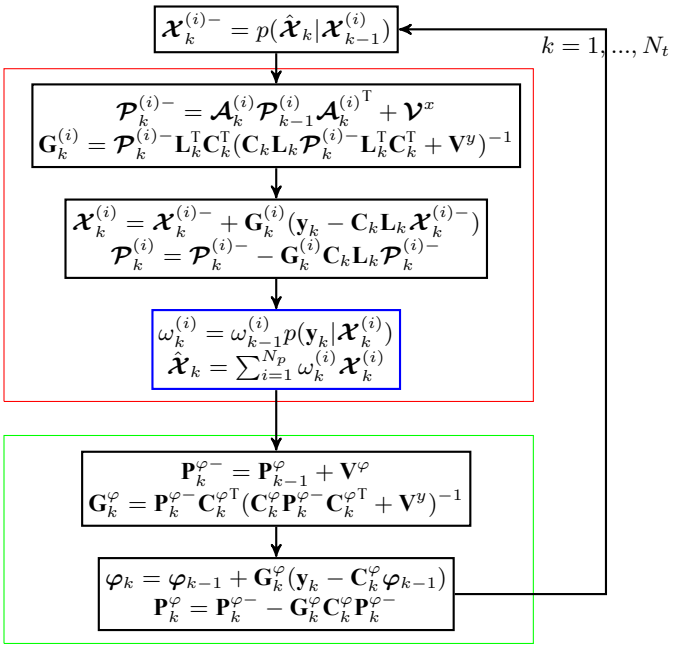

In the second stage (green box of Figure 1), the sub-space formed by the retained POMs collected in the vector $\boldsymbol{\varphi}_k$ is estimated by the Kalman filter. Here, the innovation in the update stage of the filter provides the way to catch the drift from the current structural health, and $\mathbf{V}^{\varphi}$ is the covariance of a fictitious noise added to allow POMs to evolve.

5 Results

Results are presented for a thin square plate, simply supported along its border and featuring a sidelength/thickness ratio $L/th = 40$. The structure is loaded by a sinusoidally varying force perpendicular to the mid-plane of plate, acting at its centre. The force is bounded to alleviate any damage inception and growth due to the pad itself; damage events are thus supposed to be due to other (possibly environmental) causes. Moreover, the frequency of variation of the load has been defined to avoid high frequency oscillations of the plate, but not necessarily to excite its fundamental vibration mode only.

The plate is made of a material behaving isotropically in its mid-plane, with Young's modulus $E = 70$ GPa in the virgin state and Poisson's ratio $\nu = 0.3$. As already reported in the paper, this assumption does not mean that a homogeneous and isotropic material is considered; thinking of laminated structures, this in-plane isotropy can be e.g., obtained through a wise stacking sequence of all the laminae.

In the analysis, a reference space discretisation featuring 33 finite elements along each side of the plate has been adopted. This mesh density was already proved in Mariani et al. (2015) to provide accurate results as for the whole plate kinematics, and also for the stress state if specifically designed finite elements are adopted.

In what follows, we first show the optimal deployment of the sensors, obtained thanks to the topology optimisation scheme discussed in Section 2. Next, the capability of the filtering procedure detailed in Sections 3 and 4, is checked as for the simultaneous tracking of the partially observed structural state, and identification of the local residual structural stiffness.

5.1 Optimal sensor placement

In line with the proposed topology optimisation strategy, we assume that damage can be located anywhere over the mid-plane of the plate. Such damage consists in a local reduction of the structural stiffness, which can be linked to a degradation of the material Young's modulus or to a delamination process changing the sectional moment of inertia. In the examples here shown, we have assumed that the former damage event can take place inside the structure. To understand the effectiveness of the proposed strategy, it is worth recalling that the provided placements for the sensors turn out to be well-balanced, not necessarily with the highest sensitivity to damage in the exemplary case to be considered in Section 5.2, which cannot be obviously envisioned beforehand.

Some relevant results were already reported in Bruggi and Mariani (2013) and Mariani et al. (2013a, 2014, 2015) for rectangular and square plates, with various boundary conditions along their borders. The black shaded elements in Figures 2 and 3 are those where sensors are to be placed, so where the discrete variable field in equation (1) is $x_i = 1$. For symmetry reasons and because no specific actions have been taken to penalise intermediate x_i values in the range $0 - 1$ (see Section 2), it may happen that some elements are grey shaded due to $x_i < 1$. Accordingly, they can be thought of as less important placements or, from a statistical viewpoint, as positions with a probability less than one to provide an optimal structural observation.

Figure 2 Damage in one element only; effect of the number N of sensors to be deployed on the optimal placement, (a) $N = 5$ (b) $N = 50$

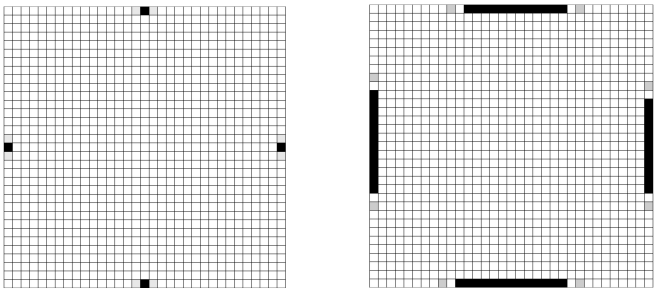

(a) (b)

Figure 3 Damage of varying size, $N = 16$; effect of damage size on the optimal placement, (a) damage in one element only (b) damage in a patch of 4×4 contiguous elements

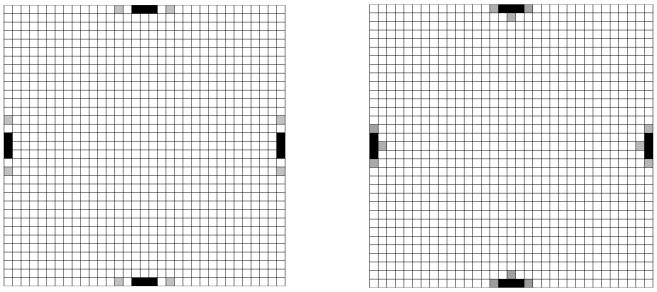

(a) (b)

Figure 2 shows results at varying value N of the sensors to be placed, a-priori defined in the analyses. Damage has been assumed to be localised in a single element, so in a region whose size corresponds to the smallest resolution of the used discretisation. Outcomes relevant to $N = 5$ and $N = 50$ are reported, but it could be shown that the deployment pattern would progressively and smoothly evolve for the values in between. It can be neatly seen that mid-points along the plate sides are a kind of accumulation points: they thus represent the best possible placement for the inertial sensors measuring the rotation of the normal to the mid-plane, induced by the loading and affected by the damage state. If N gets increased, all the sensors tend to be placed along the borders, as closer as possible to the mentioned mid-points. When the number of sensors is instead held fixed at $N = 16$, the sensor placement is depicted in Figure 3 for the two cases of damage in a single element (like in Figure 2) or in a patch of 4×4 elements. It is shown that, by increasing the size of the damaged area by a factor 4 (or by increasing its area by a factor 16), the optimal placement provided by the method is only marginally changed. This is somehow expected, since handling damage on a element-by-element basis or in patches of elements, only slightly modifies the objective function ψ in equation (1), which has been actually designed to account for all the damage pattern effects and maximise the sensitivity of the sensor network.

Independently of the damage location and amount, solutions are never given by sensors evenly spaced over the whole plate. This represents a striking strength of the

offered procedure, which is therefore able to define by itself the best regions where to place the sensors and enhance the overall sensitivity to damage of the collected measurements.

5.2 Online state tracking and damage identification

According to the problem setting depicted in Figure 4, we have assumed the plate to be sub-divided into four regions, with the damage state characterised by indices $d_1, ..., d_4$.

Figure 4 Plate geometry and notation adopted (see online version for colours)

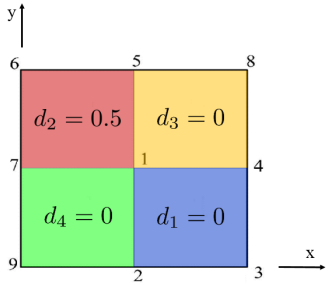

For all the analyses, only $N_p = 10$ particles have been used. In comparison with other Monte Carlo-like approaches, this strikingly low number of realisations necessary to model the evolution of statistics for the whole state vector can be already considered a strength of the proposed method. As far as the process noise covariance matrix $\boldsymbol{\mathcal{V}}^x$ is concerned, it has been assumed diagonal, with pivotal values on the order of 10^{-10} and 10^{-1} for components related to the reduced-order version of the state vector $\mathbf{x}_k$ and to the damage parameters in $\boldsymbol{\vartheta}_k$, respectively. Both values are dimensionless, as extensively discussed in Capellari et al. (2016): in fact, the former value is referred to the evolutions in time of the POMs retained in the reduced-order model, and to their time derivatives; the second one is instead linked to the range of variation $[0 \quad 1)$ of damage indices, see also Bazant and Cedolin (1991).

To assess the performance of the proposed intricate filtering procedure, we start by considering a plate affected by a time-invariant damage state with $d_2 = 0.5$, while all the other zones are damage-free. Assuming that the rotation of the plate is monitored at the four mid-points along its sides, as suggested by the maps of Section 5.1, outcomes are respectively reported in Figures 6 and 7 in terms of the tracked structural state and of the identified Young's moduli in the four regions. In the analysis, pseudo-experimental (i.e., numerically generated, fictitious) data have been adopted as structural observations at the mentioned locations; a low (almost negligible) noise level featuring $\mathbf{V}^y = \text{diag}[10^{-14}]$ (with dimensionless matrix entries, as rotations are measured in radians) has been handled in this case. Results are provided at increasing number of POMs retained in the reduced-order model during the filtering, up to $o = 3$. As far as the system evolution is concerned, in accordance with what reported in Eftekhar Azam (2014) and Capellari et al. (2016), the method is able to track with high fidelity the true, or target solution even for $o = 1$, due to the effects of the two filters that also improve the accuracy of the reduced-order model. Remarkably, not only the estimates of the observed components of the structural kinematics (the rotation at

point 5 in Figure 6), but also of the unobserved ones (the displacement and rotation at point 1, i.e., at the centre of the plate) do accurately match the target system evolution. As a result, the filter outputs are totally superposed to each other at varying o, and so plots cannot be distinguished at the scale of variation considered in the figure. Concerning the time evolution of the estimates of the stiffness parameters, Figure 7 shows instead some deficiencies of the models linked to $o = 1$ and $o = 2$. After a short transient stage moving from the initial guess (whose effect on the final results is indeed rather weak, see Capellari et al., 2016), the parameters converge towards a steady state-like solution for $o = 1$, and instead diverge after a while for $o = 2$. In the former case, the estimates provided by the filter are not accurate (the target values of E_{i} being represented by the dashed lines in these plots), since the reduced-order model is incapable of describing the plate kinematics in the damage state with a proper accuracy, and of distinguishing the effects of the stiffness of each region on the measured response to loading. In the latter case, the solution initially converges to the correct one, but then error cumulation induced by the measurement noise, although small, triggers the divergence of the estimations. For $o = 3$ the solution is instead very accurate; only some small fluctuations are shown around the target values, as induced by the noise and by the particle filtering approach (see Eftekhar Azam and Mariani, 2012), but they do not lead to divergence or bias phenomena.

Figure 5 Time-invariant damage case $d_2 = 0.5$ and $d_1 = d_3 = d_4 = 0$, high noise level (see online version for colours)

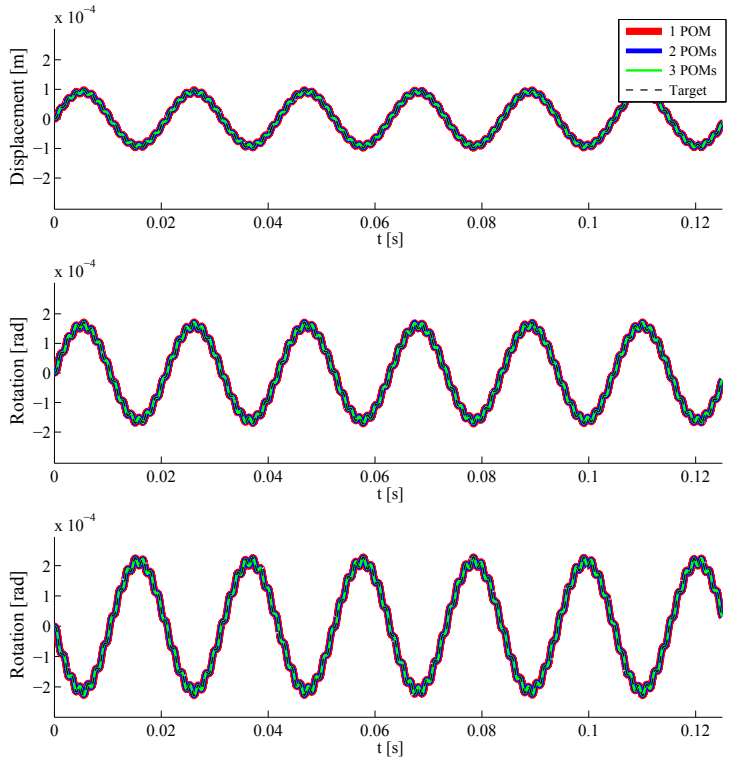

Notes: Comparison between the target system evolution and the relevant forecasts provided by the SHM procedure, at varying number of POMs retained in the reduced-order model, in terms of (from top to bottom): out-of-plane displacement at the centre of the plate; rotation about the x axis at the centre of the plate; rotation about the x axis at mid-point 5 along the plate border.

By increasing the noise level to $\mathbf{V}^y = \text{diag}[10^{-8}]$, results are reported in Figure 5 in terms of the tracked system evolution. It is shown that only the out-of-plane displacement at the centre of the plate, where load is applied, is always accurately provided by the filter, even if unobserved. Rotations are instead not well tracked with $o = 1$ or $o = 2$; if $o = 3$ the solution almost perfectly matches the target one, with an accuracy that is progressively improved over time by the filter.

Figure 6 Time-invariant damage case $d_2 = 0.5$ and $d_1 = d_3 = d_4 = 0$, low noise level (see online version for colours)

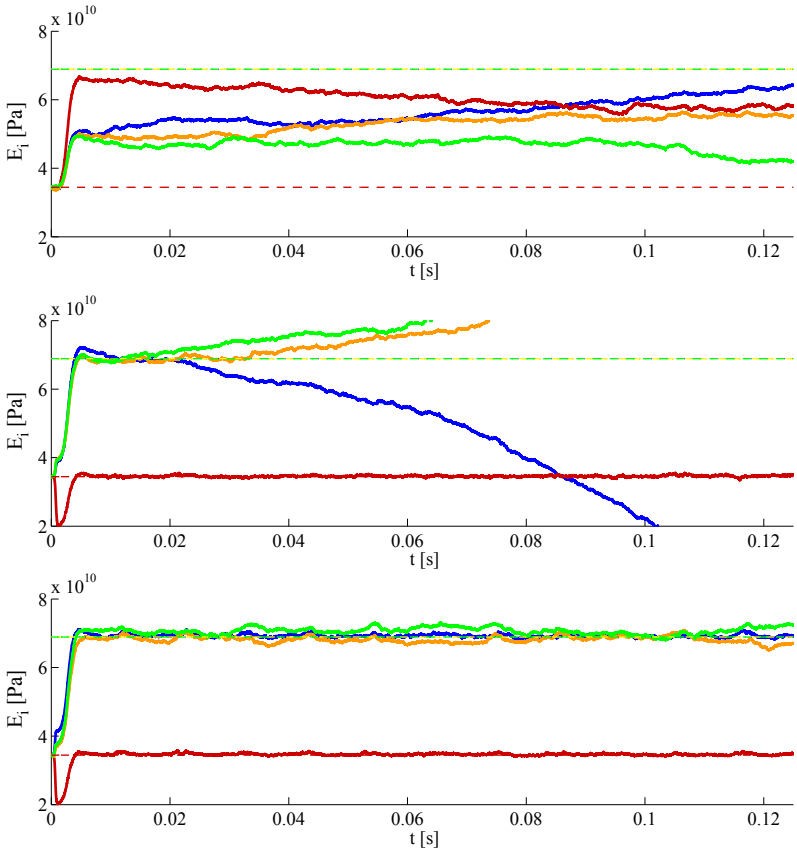

Notes: Time evolution of the estimates of the Young's moduli in the four plate regions, at varying number of POMs retained in the reduced-order model: from top to bottom $o = 1$, $o = 2$ and $o = 3$ (for colour codes, see Figure 4).

A case featuring a time-varying health state is finally considered: up to $t = 0.0375$ s the damage pattern is the same considered before; afterwards, it is assumed that damage in region #2 is suddenly increased to $d_2 = 0.7$, and that region #3 gets damaged with $d_3 = 0.2$. Such case is exemplary, and very similar results can be obtained for any other possible health evolution history. For a low noise level, Figure 8 shows the time evolution of the estimates of the Young's moduli in the four regions. At variance

with what reported in Figure 7, now the estimates do not diverge with $o = 1$ and $o = 2$; anyway, convergence towards the target values is not reported for all the four parameters. The other way around, if $o = 3$ the estimates promptly move towards the target ones and then slightly fluctuate in time. Accuracy of the results concerning state tracking turns out to be very similar to the one reported for the time-invariant damage state, and so additional plots are not reported here for brevity.

The shown fast convergence of the estimates of the local structural stiffness values towards the target ones, soon after the damage pattern has been varied, proves the capability of the proposed procedure to track in real-time the possible changing health of the structure, without delays.

Figure 7 Time-invariant damage case $d_2 = 0.5$ and $d_1 = d_3 = d_4 = 0$, low noise level (see online version for colours)

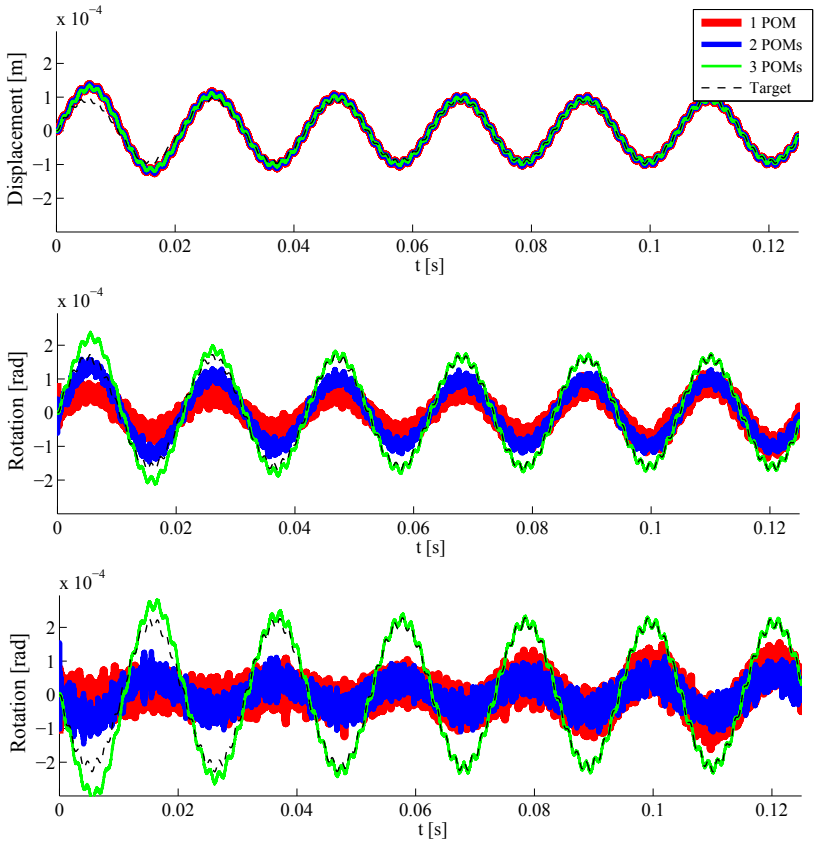

Notes: Comparison between the target system evolution and the relevant forecasts provided by the SHM procedure, at varying number of POMs retained in the reduced-order model, in terms of (from top to bottom): out-of-plane displacement at the centre of the plate; rotation about the x axis at the centre of the plate; rotation about the x axis at mid-point 5 along the plate border (see Figure 4).

Figure 8 Time-varying damage case $d_2 = 0.5$ and $d_1 = d_3 = d_4 = 0$ up to $t = 0.0375$ s, $d_2 = 0.7$, $d_3 = 0.2$ and $d_1 = d_4 = 0$ afterwards, low noise level (see online version for colours)

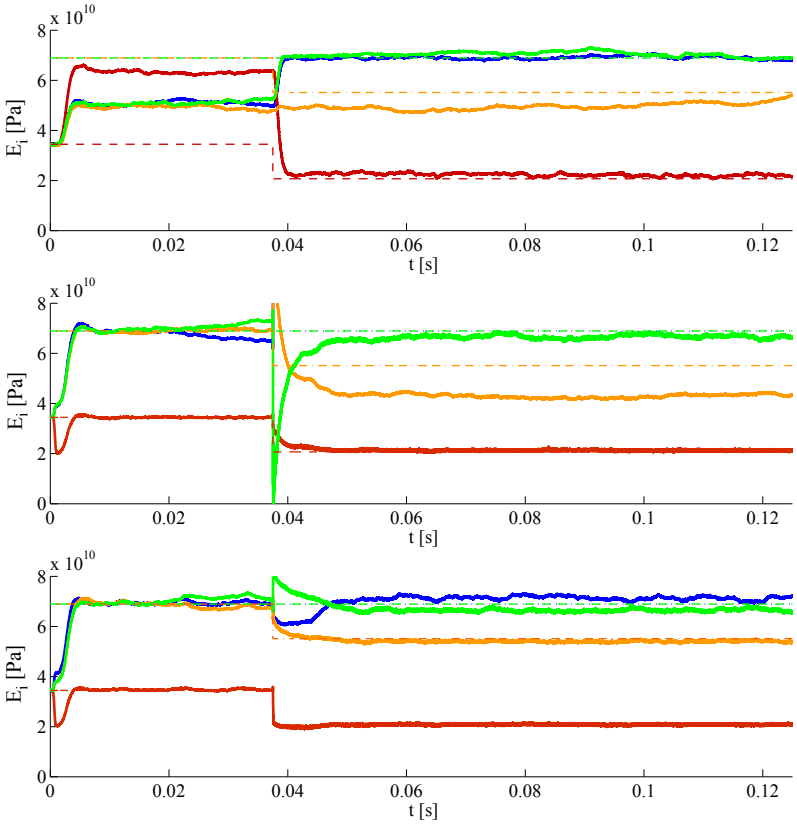

Notes: Time evolution of the estimates of the Young's moduli in the four plate regions, at varying number of POMs retained in the reduced-order model: from top to bottom $o = 1$, $o = 2$ and $o = 3$ (for colour codes, see Figure 4).

6 Conclusions

In this paper, we have discussed a general framework for the health monitoring of lightweight structures like thin composite plates. Due to their light weight, such structures can take advantage of the adoption of micro-sensors to sense their structural response to loadings. While for massive concrete or steel structures the added mass of the SHM system does not represent an issue, developing a network of sensors, whose inertia under dynamic excitations proves negligible if compared to the structural one, would be beneficial for the considered class of structures. Besides inertial MEMS, other types of sensors feature this low weight requirement; for instance, fiber sensors, to be embedded into composite laminates, may also prove efficient in this sense, but they lead to a distortion of the microstructure of the composite material that results in a possible trigger of damage events. From a reliability point of view, that would represent

a weakness of the SHM approach; we then proposed to surface-mount the micro-sensors, so as to avoid any mechanical interaction between the composite and the SHM system.

Here, we have reviewed a methodology to optimally deploy a set of inertial sensors, feeling the change of the local rotation of the plate induced by the loading and by the presence of a damage incepted anywhere in the structure, and maximising the sensitivity of the whole sensing system to the damage itself. As for the sensor placement over thin rectangular plates either simply supported or clamped along their borders, this procedure was already shown to provide outcomes independent (within reasonable bounds) of damage amplitude and loading conditions. For the specific case here considered of a square plate supported all over its border, it has been also reported that a network of evenly spaced sensors would not be optimal, as some of the devices would be placed where rotations are small due to the boundary conditions; instead, accumulation-like points have been reported close to the mid-points along plate edges.

With the goal of moving towards a real-time SHM strategy, a recursive Bayesian filter has been adopted as engine of the identification procedure, aimed to locate and quantify a possible structural damage, soon after it has been incepted. While the filter is able by itself to effectively handle the measurements gathered, and progressively improve the estimation of the damage pattern, good results can be obtained only if a sufficiently accurate model of the structure (able to capture the links between the damage process and the overall mechanical response) is used. Such model accuracy entails computational costs that almost surely prevent a real-time monitoring of real-life structures. Hence, a proper orthogonal decomposition-based reduced-order modelling of the structural system has been adopted, in conjunction with Bayesian filtering.

As already reported in some preliminary studies, see Eftekhar Azam (2014), this joint use of a filtering technique and of a reduced-order model is beneficial for SHM purposes. If features of the reduced-order model, like e.g., the proper orthogonal modes, are handled by a further Bayesian filter, the accuracy of the said reduced-order model gets increased while the damage state estimation is improved.

Results have been reported for a thin square plate, simply supported along its border. It has been assumed that damage is uniform, already present from the beginning in one quarter of the mid-plane of the plate, and can evolve in time due to some external causes, not necessarily linked to the considered loading conditions. The SHM procedure has been shown to promptly react to such evolving structural health, and to provide an accurate assessment of the damage pattern even when measurements are affected by environmental and system noises.

In future investigations, the proposed framework will be improved by accounting for additional uncertainties linked to the external excitations, now handled in a purely deterministic way, see e.g., Eftekhar Azam et al. (2015). Furthermore, an enhanced optimisation scheme allowing also for the power consumption of the whole sensor network will be proposed, so as to minimise the number of sensors to be deployed over the structure.

Acknowledgements

Giovanni Capellari and Stefano Mariani wish to acknowledge the financial support by Fondazione Cariplo through project *Safer Helmets*.

References

Abrate, S. (1998) *Impact on Composite Structures*, Cambridge University Press, Cambridge, UK.

Achenbach, J.D. (2009) 'Structural health monitoring – what is the prescription?', *Mechanics Research Communications*, Vol. 36, No. 2, pp.137–142.

Allix, O., Ladevéze, P. and Corigliano, A. (1995) 'Damage analysis of interlaminar fracture specimens', *Composite Structures*, Vol. 31, No. 1, pp.61–74.

Allix, O., Lévèque, D. and Perret, L. (1998) 'Interlaminar interface model identification and forecast of delamination in composite laminates', *Composites Science and Technology*, Vol. 58, No. 5, pp.671–678.

Arulampalam, M., Maskell, S., Gordon, N. and Clapp, T. (2002) 'A tutorial on particle filters for online nonlinear/non-Gaussian Bayesian tracking', *IEEE Transactions on Signal Processing*, Vol. 50, No. 2, pp.174–188.

Bazant, Z.P. and Cedolin, L. (1991) *Stability of Structures*, Oxford University Press, Oxford, UK.

Bruggi, M. and Mariani, S. (2013) 'Optimization of sensor placement to detect damage in flexible plates', *Engineering Optimization*, Vol. 45, No. 6, ppp.659–676.

Butler, S., Gurvich, M., Ghoshal, A., Welsh, G., Attridge, P., Winston, H., Urban, M. and Bordick, N. (2011) 'Effect of embedded sensors on interlaminar damage in composite structures', *Journal of Intelligent Material Systems and Structures*, Vol. 22, No. 16, ppp.1857–1868.

Caiazzo, A. and Costanzo, F. (2000) 'On the constitutive relation of materials with evolving microstructure due to microcracking', *International Journal of Solids and Structures*, Vol. 37, No. 24, ppp.3375–3398.

Caimmi, F., Mariani, S., De Fazio, M. and Bendiscioli, P. (2014) 'Investigation of the effectiveness and robustness of a MEMS-based structural health monitoring system for composite laminates', *IEEE Sensors Journal*, Vol. 14, No. 7, pp.2208–2215.

Capellari, G., Eftekhar Azam, S. and Mariani, S. (2016) 'Damage detection in flexible plates through reduced-order modeling and hybrid particle-Kalman filtering', *Sensors*, Vol. 16, No. 1, 2.

Chatzi, E. and Smyth, A. (2009) 'The unscented Kalman filter and particle filter methods for nonlinear structural system identification with non-collocated heterogeneous sensing', *Structural Control and Health Monitoring*, Vol. 16, No. 1, pp.99–123.

Chatzi, E. and Smyth, A. (2013) 'Particle filter scheme with mutation for the estimation of time-invariant parameters in structural health monitoring applications', *Structural Control and Health Monitoring*, Vol. 20, No. 7, pp.1081–1095.

Corigliano, A. and Mariani, S. (2002) 'Identification of a constitutive model for the simulation of time-dependent interlaminar debonding processes in composites', *Computer Methods in Applied Mechanics and Engineering*, Vol. 191, No. 17, pp.1861–1894.

Corigliano, A., Dossi, M. and Mariani, S. (2013a) 'Domain decomposition and model order reduction methods applied to the simulation of multiphysics problems in MEMS', *Computers and Structures*, Vol. 122, pp.113–127.

Corigliano, A., Dossi, M. and Mariani, S. (2013b) 'Recent advances in computational methods for microsystems', *Advanced Materials Research*, Vol. 745, pp.13–25.

Corigliano, A., Dossi, M. and Mariani, S. (2015) 'Model order reduction and domain decomposition strategies for the solution of the dynamic elasto-plastic structural problem', *Computer Methods in Applied Mechanics and Engineering*, Vol. 290, pp.127–155.

Corigliano, A. (2003) 'Damage and fracture mechanics techniques for composite structures', in I. Milne, R. Ritchie, and B. Karihaloo (Eds.): *Comprehensive Structural Integrity*, Vol. 3, Chapter 9, pp.459–539, Elsevier Science.

Costanzo, F. and Walton, J. (2002) 'Steady growth of a crack with a rate and temperature sensitive cohesive zone', *Journal of the Mechanics and Physics of Solids*, Vol. 50, No. 8, pp.1649–1679.

Douc, R. and Cappe, O. (2005) 'Comparison of resampling schemes for particle filtering', in *Proceedings of the 4th International Symposium on Image and Signal Processing and Analysis, ISPA*, pp.64–69.

Doucet, A., Godsill, S. and Andrieu, C. (2000) 'On sequential monte carlo sampling methods for bayesian filtering', *Statistics and Computing*, Vol. 10, No. 3, pp.197–208.

Eftekhar Azam, S. (2014) *Online Damage Detection in Structural Systems*, Springer, Milan, Italy.

Eftekhar Azam, S. and S.Mariani (2012) 'Dual estimation of partially observed nonlinear structural systems: a particle filter approach', *Mechanics Research Communications*, Vol. 46, pp.54–61.

Eftekhar Azam, S. and Mariani, S. (2013) 'Investigation of computational and accuracy issues in POD-based reduced order modeling of dynamic structural systems', *Engineering Structures*, Vol. 54, pp.150–167.

Eftekhar Azam, S., Chatzi, E. and Papadimitriou, C. (2015) 'A dual Kalman filter approach for state estimation via output-only acceleration measurements', *Mechanical Systems and Signal Processing*, Vol. 60, pp.866–886.

Gelb, A. (1974) *Applied Optimal Estimation*, The MIT Press, Cambridge, USA.

Hol, J., Schon, T. and Gustafsson, F. (2006) 'On resampling algorithms for particle filters', in *Nonlinear Statistical Signal Processing Workshop, IEEE*, pp.79–82.

Hull, D. and Clyne, T. (1996) *An Introduction to Composite Materials*, 2nd ed., Cambridge Solid State Science Series, Cambrige University Press, Cambridge, UK.

Julier, S., Uhlmann, J. and Durrant-Whyte, H. (1995) 'A new approach for filtering nonlinear systems', in *Proceedings of the American Control Conference*, Seattle, June, pp.1628–1632.

Julier, S., Uhlmann, J. and Durrant-Whyte, H. (2000) 'A new method for the nonlinear transformation of means and covariances in filters and estimators', *IEEE Transactions on Automatic Control*, Vol. 45, No. 3, pp.477–482.

Kalman, R.E. (1960) 'A new approach to linear filtering and prediction problems', *ASME Journal of Basic Engineering*, Vol. 82D, No. 1, pp.35–45.

Konka, H.P., Wahab, M.A. and Lian, K. (2012) 'The effects of embedded piezoelectric fiber composite sensors on the structural integrity of glass-fiber epoxy composite laminate', *Smart Materials and Structures*, Vol. 21, No. 1, 015016.

Ladevéze, P., Lubineau, G. and Marsal, D. (2006) 'Towards a bridge between the micro- and mesomechanics of delamination for laminated composites', *Composites Science and Technology*, Vol. 66, No. 6, pp.698–712.

Leng, J. and Asundi, A. (2003) 'Structural health monitoring of smart composite materials by using EFPI and FBG sensors', *Sensors and Actuators A: Physical*, Vol. 103, No. 3, pp.330–340.

Mariani, S. and Corigliano, A. (2005) 'Impact induced composite delamination: state and parameter identification via joint and dual extended Kalman filters', *Computer Methods in Applied Mechanics and Engineering*, Vol. 194, Nos. 50–52, pp.5242–5272.

Mariani, S. and Ghisi, A. (2007) 'Unscented Kalman filtering for nonlinear structural dynamics', *Nonlinear Dynamics*, Vol. 49, No. 1, pp.131–150.

Mariani, S., Bruggi, M., Caimmi, F., Bendiscioli, P. and De Fazio, M. (2013a) 'Sensor deployment over damage-containing plates: a topology optimization approach', *Journal of Intelligent Material Systems and Structures*, Vol. 24, No. 9, pp.1105–1122.

Mariani, S., Bruggi, M., Caimmi, F., Bendiscioli, P. and De Fazio, M. (2013b) 'Surface-mounted SHM system for composite structures, featuring MEMS sensors and flexible PCBs', in *Euromech Colloquium No. 541, New Advances in the Nonlinear Dynamics and Control of Composites for Smart Engineering Design*, Senigallia, Italy.

Mariani, S., Corigliano, A., Caimmi, F., Bruggi, M., Bendiscioli, P. and De Fazio, M. (2013c) 'MEMS-based surface mounted health monitoring system for composite laminates', *Microelectronics Journal*, Vol. 44, No. 7, pp.598–605.

Mariani, S., Caimmi, F., Bruggi, M. and Bendiscioli, P. (2014) 'Smart sensing of damage in flexible plates through MEMS', *International Journal of Mechanisms and Robotic Systems*, Vol. 2, No. 1, pp.67–95.

Mariani, S., Bruggi, M., Caimmi, F. and Bendiscioli, P. (2015) 'Optimal placement of mems sensors for damage detection in flexible plates', *Structural Longevity*, in press.

Melnykowycz, M. and Brunner, A.J. (2011) 'The performance of integrated active fiber composites in carbon fiber laminates', *Smart Materials and Structures*, Vol. 20, No. 7, 075007.

Mieloszyk, M., Skarbek, L., Krawczuk, M., Ostachowicz, W. and Zak, A. (2011) 'Application of fibre bragg grating sensors for structural health monitoring of an adaptive wing', *Smart Materials and Structures*, Vol. 20, No. 12, 125014.

Minakuchi, S., Tsukamoto, H., Banshoya, H. and Takeda, N. (2011) 'Hierarchical fiber-optic-based sensing system: impact damage monitoring of large-scale CFRP structures', *Smart Materials and Structures*, Vol. 20, No. 8, 085029.

Nemat-Nasser, S. and Hori, M. (1993) *Micromechanics : Overall Properties of Heterogeneous Materials*, North-Holland, Amsterdam, New York.

O'Brien, T. (1984) 'Mixed-mode strain-energy-release rate effects on edge delamination of composites', in *Effects of Defects in Composite Materials, ASTM STP 836*, American Society for Testing and Materials, pp.125–142.

Orlowska, A., Kolakowski, P. and Holnicki-Szulc, J. (2011) 'Detecting delamination zones in composites by embedded electrical grid and thermographic methods', *Smart Materials and Structures*, Vol. 20, No. 10, 105009.

Ratcliffe, C., Heider, D., Crane, R., Krauthauser, C., Yoon, M.K. and Gillespie Jr., J.W. (2008) 'Investigation into the use of low cost MEMS accelerometers for vibration based damage detection', *Composite Structures*, Vol. 82, No. 1, pp.61–70.

Reddy, J. (2004) *Mechanics of Laminated Composite Plates and Shells: Theory and Analysis*, CRC Press, Boca Raton, FL, USA.

Sirovich, L. (1987) 'Turbulence and the dynamics of coherent structures. I – coherent structures. II – symmetries and transformations. III – dynamics and scaling', *Quarterly of Applied Mathematics*, Vol. 45, No. 3, pp.561–590.

Sohn, J., Choi, S-B. and Kim, H. (2011) 'Vibration control of smart hull structure with optimally placed piezoelectric composite actuators', *International Journal of Mechanical Sciences*, Vol. 53, No. 8, pp.647–659.

Tang, H-Y., Winkelmann, C., Lestari, W. and La Saponara, V. (2011) 'Composite structural health monitoring through use of embedded PZT sensors', *Journal of Intelligent Material Systems and Structures*, Vol. 22, No. 8, pp.739–755.

Yu, C., Pandolfi, A., Ortiz, M., Coker, D. and Rosakis, A. (2002) 'Three-dimensional modeling of intersonic shear-crack growth in asymmetrically loaded unidirectional composite plates', *International Journal of Solids and Structures*, Vol. 39, pp.6135–6157.

Zhuang, S., Ravichandran, G. and Grady, D. (2003) 'An experimental investigation of shock wave propagation in periodically layered composites', *Journal of the Mechanics and Physics of Solids*, Vol. 51, No. 2, pp.245–265.

Zienkiewicz, O.C. and Taylor, R.L. (2000) *The Finite Element Method: The Basis*, 5th ed., Vol. 1, Butterworth-Heinemann, Oxford, UK.